


# Vascular targeting of LIGHT normalizes blood vessels in primary brain cancer and induces intratumoural high endothelial venules

Bo He<sup>1</sup>, Arnaud Jabouille<sup>2</sup>, Veronica Steri<sup>2</sup>, Anna Johansson-Percival<sup>1</sup>, Iacovos P Michael<sup>3</sup>, Venkata Ramana Kotamraju<sup>4</sup>, Reimar Junckerstorff<sup>5,6</sup>, Anna K Nowak<sup>7</sup>, Juliana Hamzah<sup>1</sup>, Gabriel Lee<sup>8,9</sup>, Gabriele Bergers<sup>2,10</sup> and Ruth Ganss<sup>1\*</sup> 

<sup>1</sup> The Harry Perkins Institute of Medical Research, Centre for Medical Research, University of Western Australia, Nedlands, Australia

<sup>2</sup> Department of Neurological Surgery, Brain Tumour Research Center, Helen Diller Family Comprehensive Cancer Center, University of California, San Francisco, CA, USA

<sup>3</sup> Swiss Institute for Experimental Cancer Research, School of Life Sciences, Swiss Federal Institute of Technology Lausanne (EPFL), Lausanne, Switzerland

<sup>4</sup> Cancer Research Center, Sanford Burnham Prebys Medical Research Institute, La Jolla, CA, USA

<sup>5</sup> School of Pathology and Laboratory Medicine, University of Western Australia, Nedlands, Australia

<sup>6</sup> PathWest Neuropathology, Royal Perth Hospital, Perth, Australia

<sup>7</sup> School of Medicine, University of Western Australia, Nedlands, Australia

<sup>8</sup> School of Surgery, University of Western Australia, Nedlands, Australia

<sup>9</sup> St John of God Subiaco Hospital, Subiaco, Australia

<sup>10</sup> VIB Centre for Cancer Biology Vesalius and Department of Oncology, KU Leuven, Leuven, Belgium

\*Correspondence to: R Ganss, The Harry Perkins Institute of Medical Research, 6 Verdun Street, Nedlands, Western Australia 6009, Australia.  
E-mail: ganss@perkins.uwa.edu.au

## Abstract

High-grade brain cancer such as glioblastoma (GBM) remains an incurable disease. A common feature of GBM is the angiogenic vasculature, which can be targeted with selected peptides for payload delivery. We assessed the ability of micelle-tagged, vascular homing peptides RGR, CGKRK and NGR to specifically bind to blood vessels in syngeneic orthotopic GBM models. By using the peptide CGKRK to deliver the tumour necrosis factor (TNF) superfamily member LIGHT (also known as TNF superfamily member 14; TNFSF14) to angiogenic tumour vessels, we have generated a reagent that normalizes the brain cancer vasculature by inducing pericyte contractility and re-establishing endothelial barrier integrity. LIGHT-mediated vascular remodelling also activates endothelia and induces intratumoural high endothelial venules (HEVs), which are specialized blood vessels for lymphocyte infiltration. Combining CGKRK–LIGHT with anti-vascular endothelial growth factor and checkpoint blockade amplified HEV frequency and T-cell accumulation in GBM, which is often sparsely infiltrated by immune effector cells, and reduced tumour burden. Furthermore, CGKRK and RGR peptides strongly bound to blood vessels in freshly resected human GBM, demonstrating shared peptide-binding activities in mouse and human primary brain tumour vessels. Thus, peptide-mediated LIGHT targeting is a highly translatable approach in primary brain cancer to reduce vascular leakiness and enhance immunotherapy.

Copyright © 2018 Pathological Society of Great Britain and Ireland. Published by John Wiley & Sons, Ltd.

**Keywords:** angiogenesis; vascular targeting; LIGHT; TNFSF14; glioblastoma; immunotherapy

Received 6 December 2017; Revised 21 February 2018; Accepted 20 March 2018

No conflicts of interest were declared.

## Introduction

World Health Organization (WHO) grade IV glioma [glioblastoma (GBM)] is a highly aggressive malignancy and the most common form of primary human brain cancer. Standard treatment for GBM includes surgical resection followed by radiation, and has remained unchanged for decades; the recent addition of concurrent and adjuvant chemotherapy with temozolomide only marginally improved the poor survival outcomes. GBM is a highly angiogenic tumour, in part because of elevated levels of vascular endothelial

growth factor (VEGF). Features of abnormal angiogenesis, leaky blood vessels and irregular blood flow create a hypoxic tumour environment, high interstitial fluid pressure, and brain oedema [1]. Cancer-associated oedema and the use of corticosteroids for treatment contribute to overall patient morbidity, and constitute a serious clinical problem [2]. Pharmacological inhibition of VEGF by bevacizumab has been Food and Drug Administration-approved since 2009, but thus far has not clearly delivered survival benefits [3,4]. More recently, it has been demonstrated that therapeutic resistance following prolonged VEGF blockade and

vessel destruction is associated with increased tumour hypoxia, invasive cancer growth, and mobilization of innate immune cells into the tumour environment [5–7]. Nevertheless, anti-angiogenic therapy can induce a transient state of vessel ‘normalization’ that improves tumour perfusion and alleviates brain oedema, and thus provides a temporary opportunity for drug delivery [8]. In normalized tumour blood vessels, endothelial cells and surrounding support cells, so-called pericytes, are better aligned, leading to a tighter, less leaky and more functional vasculature [9,10]. Although there is currently no single reagent that can induce long-lasting vessel normalization, clinical data from anti-VEGF treatment, in particular in GBM, support the notion that vessel normalization might be therapeutically beneficial [8,11].

To specifically deliver payloads to the angiogenic vasculature, a variety of peptides have been identified that bind to abnormal tumour blood vessels [12–14]. Among these vascular targeting peptides (VTPs) is the so-called RGR peptide (CRGRRST), which has been identified in a preclinical model of pancreatic neuroendocrine tumours and also binds to blood vessels in breast cancer [10,15]. Other peptides, such as CGKRRK and the NGR peptide (CNGRRCG), bind to tumour blood vessels in murine breast, melanoma, squamous cell carcinoma and brain cancer models [16–19]. Thus far, NGR is the only VTP that has advanced into clinical trials to deliver the anti-angiogenic agent tumour necrosis factor (TNF)- $\alpha$  into end-stage malignancies [20,21].

We have recently developed a compound that combines a VTP with the TNF superfamily cytokine LIGHT (also known as TNFSF14), called LIGHT–VTP [10]. LIGHT is a ligand for lymphotoxin  $\beta$  receptor (LT $\beta$ R) and herpes virus entry mediator, and stimulates T cells, promotes vascular inflammation, and is involved in lymph node neogenesis [22–24]. When targeted to angiogenic blood vessels in preclinical models of neuroendocrine pancreatic or breast cancers, LIGHT normalizes the tumour vasculature and also induces specialized endothelial cells, so-called high endothelial venules (HEVs) [10,25]. HEVs express peripheral node addressin (PNAd) and facilitate lymphocyte trafficking into secondary lymphoid organs [26]. In cancer, HEVs can arise spontaneously, and are often associated with better clinical outcome [27,28]. Importantly, therapeutic induction of HEVs in solid cancers increases spontaneous antitumour immunity and enhances active immunotherapy [25,29].

We hypothesized that LIGHT–VTP treatment may induce angiogenic vessel remodelling in GBM, with potential future applications for oedema alleviation and combination immunotherapies [30]. Here, we evaluated vascular peptide binding in two distinct orthotopic murine brain tumour models, and LIGHT–VTP-induced stromal remodelling *in vivo*. Furthermore, we assessed vascular peptide binding capacities in different types of human brain malignancies in order to inform potential clinical translation of the LIGHT–VTP technology.

## Materials and methods

### Cell lines, mouse models, and human specimens

NSCG cells [Ink4/Arf-deficient neural stem cells expressing the EGFRvIII mutant of human epidermal growth factor receptor (EGFR), kindly provided by J. Phillips, University of California, San Francisco, CA, USA] [31] were cultured in Minimum Essential Medium Alpha supplemented with 20% fetal bovine serum, 100 units/ml penicillin/100  $\mu$ g/ml streptomycin, 10 mM HEPES, and 0.5% glucose. NFpp10 cells (generated from embryonic C57BL/6 neural stem cells transfected with shP53-shNF1 and shPTEN lentiviral constructs and enhanced green fluorescent protein [32]) were grown in Ham’s F12 Medium supplemented with N-2 Supplement (Thermo Fisher Scientific, Waltham, MA, USA), 20 ng/ml fibroblast growth factor-2 (Preprotech, Rocky Hill, NJ, USA), 20 ng/ml epidermal growth factor (Promega, Madison, WI, USA), 50  $\mu$ g/ml heparin (Sigma-Aldrich, St Louis, MO, USA), 2 mM L-glutamine, and 100 units/ml penicillin/100  $\mu$ g/ml streptomycin. Intracranial murine tumours were generated by implanting  $3 \times 10^5$  NSCG cells in 2.5  $\mu$ l of phosphate-buffered saline (PBS) into 4–5-week-old male and female FvBN Rag-deficient mice, or by injecting  $2 \times 10^5$  NFpp10-GBM cells into 6–8-week-old male and female C57BL/6 mice, as described previously [33]. All animal studies were approved by the University of California, San Francisco Institutional Animal Care and Use Committee. Fresh human WHO grade IV astrocytomas and grade I meningiomas were collected with patient consent at the time of surgical resection and frozen in OCT compound. All human studies were approved by the Sir Charles Gairdner Group and St John of God Health Care Human Research Ethics Committees, Western Australia, Australia (2015-084).

### Peptide synthesis

Linear peptides were synthesized as described previously [34], and labelled with 5(6)-carboxyfluorescein (FAM) separated by a 6-aminohexanoic acid spacer.

### Micelle synthesis

Peptide-tagged micelles were prepared as described previously [35]. Lipids were purchased from Avanti Polar Lipids (Alabaster, AL, USA). 1,2-Distearoyl-*sn*-glycero-3-phosphoethanolamine (PE)-*N*-(polyethylene glycol)<sub>2000</sub> (DSPE-PEG<sub>2000</sub>) was either labelled with FAM or tagged to FAM-labelled peptides, including RGR (FAM-X-CRGRRST), CGKRRK (FAM-X-CGKRRK) or NGR (FAM-X-CNGRRCG), by coupling the FAM-cysteine or cysteine on the N-terminus of the peptide to 1,2-distearoyl-*sn*-glycero-3-PE-*N*-maleimide(polyethylene glycol)<sub>2000</sub> (DSPE-PEG<sub>2000</sub>-maleimide) at a 2:1 molar ratio. The coupling reaction was performed at room temperature for a minimum of 4 h under gentle rotation, and the

reaction mixture was then dialysed in three changes of degassed water and lyophilized. 18:0 PEG<sub>2000</sub>-PE and DSPE-PEG<sub>2000</sub>-FAM or FAM-peptides were dissolved in chloroform/methanol (3:1, v/v) in a glass vial at 0.7:0.3 molar ratios. A lipid film was created manually by gentle rotation of the lipid mixture under flow of nitrogen gas to evaporate the solvent. The dried lipid film was redissolved in degassed PBS at 50 °C, vortexed, and sonicated in a waterbath sonicator (Elmasonic SH40; ELMA Ultrasonic, Singen, Germany) for 20 min at 50 °C. A final product of micelle solution <12–15 nm in diameter was generated, as measured by dynamic laser light scattering (refractive index, 1.59; viscosity, 0.89) on a Malvern Zetasizer Nano (Malvern Paralytical, Almelo, The Netherlands). The micelle solution was sequentially filtered through 0.2- $\mu$ m and 0.1- $\mu$ m filters and stored for up to 2 weeks at 4 °C until further use. Micelles were sonicated for 1 min prior to use.

### Production of LIGHT-VTP

Sequences for recombinant murine LIGHT (amino acids 58–220, 17 kDa) with C-terminal CGKRK were cloned into a modified pET-44a plasmid that contains a tobacco etch virus (TEV) cleavage site (kindly provided by E. Ingley, Harry Perkins Institute, Netherlands Western Australia, Australia). Biologically active LIGHT-CGKRK was produced as described previously [25]. In brief, LIGHT-CGKRK-expressing pET-44a/TEV plasmids were transfected into *Escherichia coli* (Rosetta) for optimal protein expression. After isopropyl- $\beta$ -D-galactopyranoside induction for 6 h at 22 °C in the presence of 5 mM EGTA, cultures were pelleted by centrifugation at 4000g for 20 min, resuspended in lysis buffer [50 mM NaH<sub>2</sub>PO<sub>4</sub>, 300 mM NaCl, 10 mM imidazole, 1 mM dithiothreitol, 1 mM phenylmethanesulfonyl fluoride (PMSF), 1 mM EDTA/EGTA, 1% Triton X-100, protease inhibitor cocktail (Sigma-Aldrich, Castle Hill, New South Wales, Australia), and 1  $\mu$ g/ml pepstatin (Calbiochem, Merck, Bayswater, Victoria, Australia), pH 8.0], and this was followed by sonication, and subsequent purification with Ni-NTA beads (Qiagen, Chadstone, Victoria, Australia). Recombinant fusion protein was dialysed overnight at 4 °C in Tris buffer (50 mM Tris, 1 mM EDTA, 1 mM EGTA, pH 8.0). The Nus•Tag/His•Tag was cleaved with TEV protease (Thermo Fisher Scientific Australia, Scoresby, Victoria, Australia) for 90 min at 30 °C. After cleavage, LIGHT-CGKRK was repurified with Ni-NTA beads in the presence of protease inhibitors (1 mM PMSF, 1 mM EDTA, 1 mM EGTA, 1  $\mu$ g/ml pepstatin, and protease inhibitor cocktail), salts (50 mM NaH<sub>2</sub>PO<sub>4</sub>, 300 mM NaCl, 10 mM imidazole) and 0.005% bovine serum albumin. Purity was assessed on Coomassie Brilliant Blue-stained protein gels, and the concentration was determined by measuring protein intensity in comparison with a band of similar size and known concentration. Endotoxin levels were determined as <0.01 EU per 1  $\mu$ g of protein with the Limulus

Amebocyte Lysate (LAL) method (LAL Chromogenic Endotoxin Quantitation Kit; Thermo Fisher Scientific, Australia).

### Treatment of tumour-bearing mice

For peptide homing studies, mice were intravenously injected 2 weeks after tumour implantation with one dose of 1 mM FAM-peptide-tagged micelles in 100  $\mu$ l or PBS vehicle. Mice were killed after 2 h, and tissue was frozen in OCT compound. For LIGHT-VTP therapy, mice were treated from day 9 after tumour implantation with biweekly injections of 20 ng recombinant LIGHT-CGKRK intravenously for 2 weeks. In combination therapies, mice were treated with LIGHT-CGKRK and biweekly intraperitoneal injections of 15 mg/kg of the anti-mouse VEGF B20 biosimilar (B20S) [29] and 10 mg/kg anti-programmed death-ligand 1 (PD-L1) (BE0101; BioXcell, West Lebanon, NH, USA) for 2 weeks. At end-stage, mice were anaesthetized and heart-perfused with 2% formalin. Some mice were injected with pimonidazole (60 mg/kg, circulated for 50–60 min; Hypoxyprobe-1 Kit; Hypoxyprobe, Burlington, MA, USA). Tissues were submerged in 10% sucrose for 2 h, incubated in 30% sucrose overnight and frozen in OCT compound.

### Immunohistochemistry

Frozen 7- $\mu$ m-thick sections were fixed in ice-cold acetone prior to immunohistochemistry (IHC). FAM-labelled micelles were detected directly on sections by the use of fluorescence microscopy without amplification. Where indicated, FAM signals were amplified with anti-fluorescein isothiocyanate (FITC) antibody (goat polyclonal ab6655, 1:300; Abcam, Cambridge, UK) followed by anti-goat IgG (H+L)-cyanin 3 (Cy3) (305-165-003, 1:3000; Jackson ImmunoResearch, West Grove, PA, USA) or anti-goat IgG (H+L)-AF488 (donkey polyclonal, ab150129, 1:2000; Abcam). The following primary antibodies were used: anti-caldesmon (E89, 1:100; Abcam), anti-calponin (EP7998Y, 1:100; Abcam), anti-CD3 (rabbit polyclonal ab5690, 1:100; Abcam), anti-CD4 [GK1.5, 1:50; Becton Dickinson (BD), North Ryde, New South Wales, Australia], anti-CD8 (Ly-2, 1:50; BD), anti-CD13 (R3-63, 1:100; Bio-Rad, Gladesville, New South Wales, Australia), anti-CD31 or anti-CD31-biotin (MEC13.3, 1:100; BD), anti-collagen I (rabbit polyclonal, pAB13488, 1:100; Abnova, Taipei City, Taiwan), anti-desmin [D33, 1:25; Abcam, amplified with the mouse on mouse kit M.O.M. (Vector, Burlingame, CA, USA)], anti-FoxP3 (FJK-16 s, 1:100; eBioscience, Scoresby, Victoria, Australia), anti-GrzB [rabbit polyclonal, P1-26616, 1:100; Invitrogen, Scoresby, Victoria, Australia, amplified with the TSA Cy3 System (Perkin Elmer, Melbourne, Victoria, Australia)], anti-intercellular adhesion molecule-1 (ICAM-1) (3E2B, 1:100; Invitrogen), anti-PNAd (MECA79, 1:50; BD), anti- $\alpha$ -smooth muscle actin ( $\alpha$ -SMA)-FITC (1A4, 1:100; Sigma-Aldrich



Australia, amplified with the M.O.M kit, Vector), anti-vascular cell adhesion molecule-1 (VCAM-1) (429, 1:100; eBioscience), and anti-vascular endothelial cadherin (VE-cadherin)/CD144 (11D4.1, 1:100; BD). Primary antibodies were detected with anti-rat IgG (H+L)-Cy3 (112-165-003, 1:3000; Jackson ImmunoResearch), anti-rabbit IgG (H+L)-Cy3 (111-166-003, 1:3000; Jackson ImmunoResearch), streptavidin-Cy3 (016-160-084, 1:3000; Jackson ImmunoResearch), or anti-rat IgG (H+L)-7-amino-4-methylcoumarin-3-acetic acid (112-155-003, 1:200; Jackson ImmunoResearch). 4',6-Diamidino-2-phenylindole (DAPI) was used in some tumours to visualize cell nuclei. Hypoxia was quantified in mice treated with pimonidazole by the use of anti-pimonidazole antibodies, according to the manufacturer's instructions (Hypoxyprobe-1 Kit; Hypoxyprobe). Assessment of perfusion by the use of lectin (Vector) was performed as previously described [36]. Human fresh frozen tumours were sectioned (7 µm), fixed in ice-cold acetone, and incubated at room temperature with 100 µl of 2 µM FAM-labelled peptide solution in PBS for 60 min; this was followed by three 5-min washes in PBS. Sections were stained for the vascular markers CD105 (SN6h, 1:100; Dako, Mulgrave, Victoria, Australia) or CD13 (WM15, 1:100; Abcam). FAM-labelled peptides were either directly detected or amplified as described above for FAM-peptide-tagged micelles. A Nikon C2si confocal microscope and NIS software (Nikon, Rhodes, New South Wales, Australia, version 4.5) were used to image lectin. A Nikon Ti-E microscope and NIS software (Nikon, version 4.0) were used for all other imaging. At least three mice or tumours were analysed per treatment group unless indicated otherwise; 5–15 images per tumour were analysed. Vessel diameter was calculated by dividing vessel area by vessel length, as described previously [10].

### Statistical analysis

Data are presented as mean ± standard error of the mean. Numbers (*n*) of mice or tumours per group and *P* values are shown in the figure legends. For comparison of cell numbers/percentages between histological groups, one-way ANOVA or two-tailed unpaired Student's *t*-tests were used, as indicated in the figure legends. *P* values of <0.05 were considered to be significant. GraphPad Prism software (version 5; GraphPad Software, La Jolla, CA, USA) was used for statistical analyses.

## Results

### VTPs bind to angiogenic blood vessels in murine GBM models

To assess the capacity of selected VTPs (RGR, CGKRK, and NGR) to bind to angiogenic blood vessels in brain tumours, we employed two clinically relevant orthotopic GBM models. NSCG tumour cells express a constitutively active mutant human epidermal growth factor

receptor (EGFRVIII) in INK4/Arf-deficient neural stem cells, and were implanted into immunocompromised mice [31]. NFpp10-GBM tumours, derived from C57BL/6 p53/PTEN-deficient neural stem cells, were grown orthotopically in syngeneic C57BL/6 hosts [29]. Two weeks after intracranial implantation, mice were injected intravenously with lipid micelles (size: 12–15 nm) containing FAM or FAM-labelled peptides (Figure 1A). *In vivo* binding of micelles to tumour blood vessels was analysed by IHC after 2 h of circulation. Our results demonstrated that peptide-loaded micelles are able to pass through the circulation into brain tumours and bind specifically to the angiogenic vasculature but not to normal vessels (Figure 1B–D). In both brain tumour models (NSCG-GBM and NFpp10-GBM), >80% of CD31-positive tumour blood vessels were covered with CGKRK-FAM-loaded micelles. RGR micelles bound to 30–40% of tumour vessels, whereas NGR micelle binding was undetectable by direct visualization of fluorescent signals or after signal amplification with an anti-FITC antibody (Figure 1B,C; supplementary material, Figure S1A). This is consistent with the presence of the NGR receptor aminopeptidase N/CD13 on normal brain vessels [37] but its absence in mouse brain tumours (supplementary material, Figure S1B). Thus, CGKRK was the best-performing peptide for payload delivery into highly angiogenic GBM models that closely resemble human GBM.

### LIGHT–CGKRK treatment normalizes angiogenic blood vessels and induces pericyte phenotype switching

Given the strong and specific CGKRK coverage of angiogenic GBM blood vessels as compared with RGR or NGR peptides, we used recombinant DNA technology to produce LIGHT–CGKRK consisting of murine LIGHT<sub>58–220</sub> fused with the C-terminus of CGKRK. Mice harbouring established NFpp10-GBM tumours were treated with intravenous injections of LIGHT–CGKRK fusion compound twice weekly for 2 weeks (Figure 2A), and this was followed by histological analysis of tumour stroma. LIGHT–VTP therapy at a dose of 20 ng per mouse (≈600 ng/kg body weight) significantly reduced tumour vessel length and diameter as compared with untreated GBM, to a level resembling the calibre of normal brain capillaries (Figure 2B–D). Importantly, overall vascularity was not reduced, indicating that single LIGHT–CGKRK treatment did not destroy tumour vessels (Figure 2E). To further assess the potential of LIGHT–CGKRK to 'normalize' or 'tighten' the leaky brain tumour vasculature, we first focused on pericytes, which constitute the outer layer of blood vessels. LIGHT–VTP treatment did not change the number of pericytes that were attached to endothelial cells as compared with untreated tumours, as shown by quantification of desmin-positive pericytes surrounding CD31<sup>+</sup> tumour blood vessels (Figure 3A). We recently discovered, in a mouse model of neuroendocrine pancreatic cancer, that pericytes, much like their close

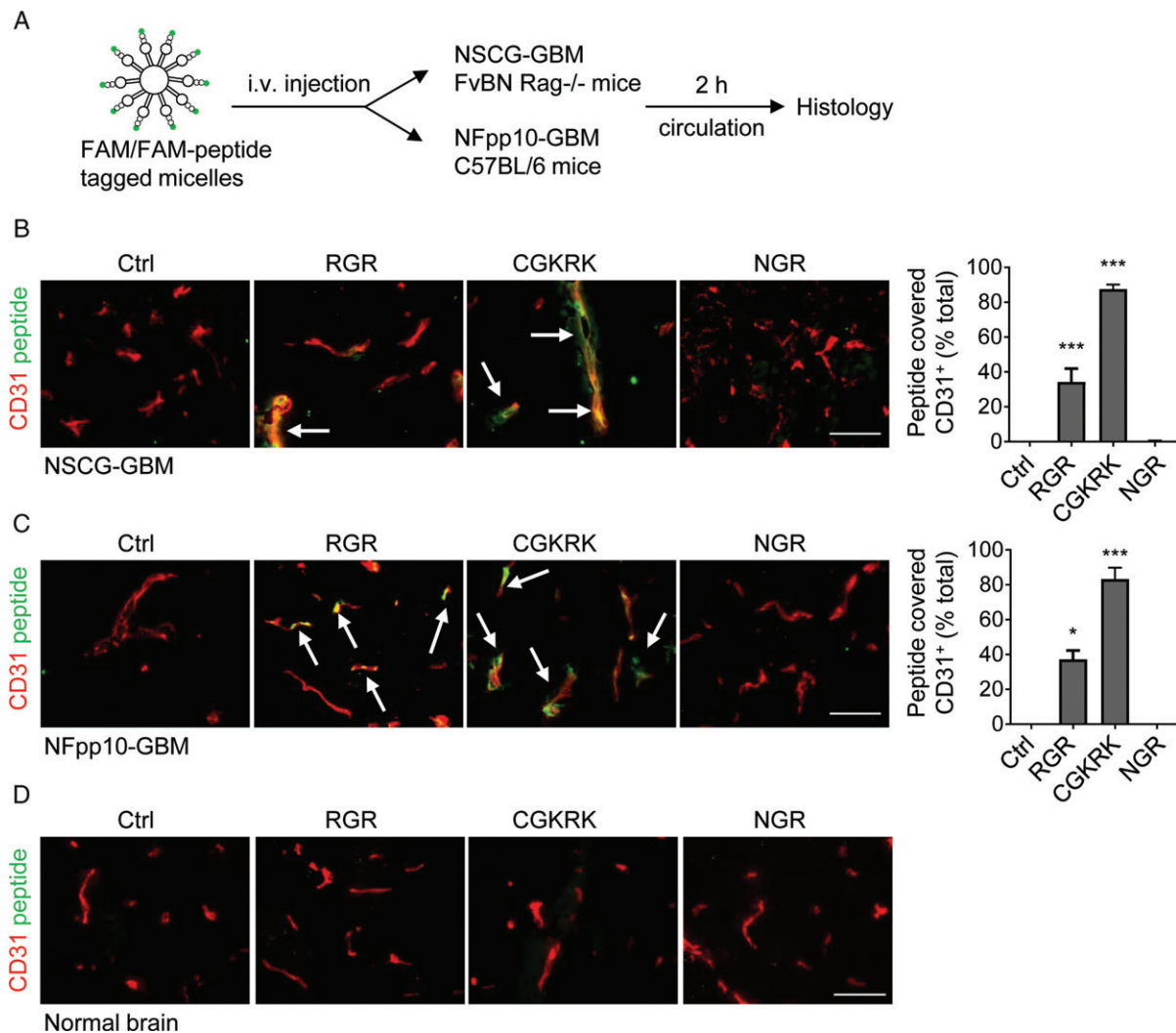


**Figure 1.** CGK RK peptide has high binding affinity for angiogenic blood vessels in orthotopic GBM models. (A) Treatment scheme of mice bearing NSCG-GBMs or NFpp10-GBMs with peptide-tagged micelles. (B) Immunohistochemical analysis of NSCG-GBM after micelle injection. FAM-labelled micelles were injected without peptide (control, Ctrl) or tagged with RGR-FAM, CGK RK-FAM or NGR-FAM peptides (green), and peptide-covered (yellow) CD31<sup>+</sup> (red) tumour vessels were quantified;  $n = 2$ , 200–400 blood vessels/mouse, \*\*\* $p < 0.0001$ . (C) Quantitative analysis of peptide-loaded micelles in relation to blood vessels in NFpp10-GBM as in (B);  $n = 2$  mice/group, 200–400 blood vessels/mouse. \* $p = 0.022$ , \*\*\* $p < 0.0001$ , ANOVA. Arrows point to some blood vessels with bound peptides. (D) Representative images of FAM-peptide homing to normal brain (control). Scale bars: 50  $\mu\text{m}$ . i.v., intravenous.

relatives the vascular smooth muscle cells, can switch from an angiogenic, proliferative or synthetic phenotype to a more quiescent, contractile and mature state [10]. To assess the maturation state of brain tumour pericytes, we quantified the contractile markers  $\alpha$ -SMA, calponin, and caldesmon, as well as the synthetic marker collagen I, in tumour blood vessels before and after therapy. Under LIGHT-VTP treatment, all contractile markers were significantly upregulated, whereas synthesis of the extracellular matrix marker collagen I was reduced (Figure 3B–E). This indicates that pericytes become more mature during LIGHT-CGK RK treatment as part of brain tumour vessel normalization.

#### LIGHT-CGK RK treatment improves vessel function and activates endothelia

Normalization of the angiogenic tumour vasculature comprises qualitative changes in pericytes and

endothelial cells [9]. In particular, VE-cadherin, a component of endothelial cell-to-cell adherens junctions, contributes to the re-establishment of vessel integrity, and is upregulated during endothelial normalization in a variety of tumour models [38–40]. We found that, in NFpp10-GBM treated with LIGHT-CGK RK for 2 weeks, VE-cadherin expression was upregulated as compared with untreated controls and signals were less disjointed (Figure 4A). This is also consistent with more continuous and tighter adherens junctions induced by LIGHT in endothelial cells *in vitro* [25]. Importantly, enhanced pericyte contractility (Figure 3) and endothelial barrier function correlated with improved tumour perfusion as shown by reduced intratumoural hypoxia (Figure 4B) and enhanced lectin binding to tumour vessels (supplementary material, Figure S2) in LIGHT-CGK RK-treated mice as compared with untreated mice. Moreover, ICAM-1 and VCAM-1, which are markers for activated endothelium, were

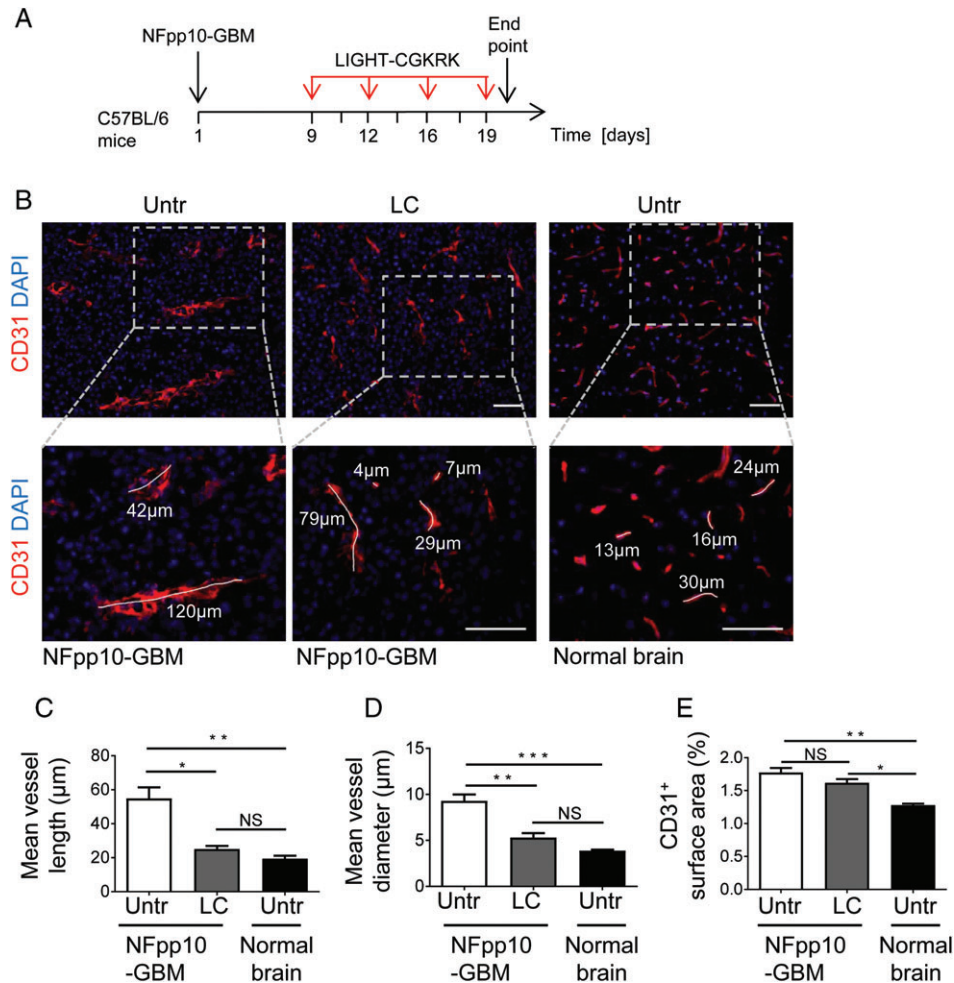


**Figure 2.** *In vivo* LIGHT–CGKRK treatment normalizes GBM blood vessels. (A) LIGHT–CGKRK treatment scheme in C56BL/6 mice harbouring established NFpp10–GBM. (B) Representative IHC of blood vessels (CD31, red) in untreated brain tumours (NFpp10–GBM, Untr), NFpp10–GBM mice treated with four intravenous injections of 20 ng of LIGHT–CGKRK (LC), or normal brain from untreated mice. Dashed outlines indicate the areas enlarged below. Two to four representative vessels per group are demarcated to indicate vessel size. Scale bars: 50 μm. (C–E) Quantification of (C) mean vessel length ( $n = 3$ ,  $*p = 0.005$ ,  $**p = 0.002$ ), (D) mean vessel diameter ( $n = 3$ ,  $**p = 0.003$ ,  $***p = 0.0006$ ) and (E) overall vascularity (CD31<sup>+</sup> surface area) ( $n = 3$ ,  $*p = 0.01$ ,  $**p = 0.002$ ) in treatment groups as described in (B). ANOVA. NS, not statistically significant.

upregulated in LIGHT–CGKRK-treated murine GBM (Figure 4C,D). Re-expression of adhesion molecules on angiogenic blood vessels together with improved intratumoural blood flow may, in turn, facilitate leukocyte transmigration into brain tumours [36,41–43].

#### LIGHT–CGKRK induces HEV formation and lymphocyte accumulation in murine GBM

To assess whether LIGHT–CGKRK treatment increases spontaneous T-cell infiltration, NFpp10-GBM mice were treated with 20 ng LIGHT–CGKRK for 2 weeks, and tumours were analysed for expression of the HEV/PNAd marker MECA79 (Figure 5A). Whereas naive NFpp10-GBM brain tumours did not harbour HEVs (Figure 5B), 20% of CD31<sup>+</sup> blood vessels in LIGHT–CGKRK-treated brain tumours were positive for MECA79 (Figure 5B), indicating substantial angiogenic vessel reprogramming but no reduction in overall vascularity (Figure 5B). Furthermore, untreated NFpp10-GBMs were sparsely infiltrated by CD3<sup>+</sup> T

cells (Figure 5C) that did not cluster around CD31<sup>+</sup> blood vessels (supplementary material, Figure S3, left). Following LIGHT–CGKRK treatment, significantly more CD3<sup>+</sup> immune cells had infiltrated the brain tumours ( $p = 0.023$ ; Figure 5C) and specifically accumulated around HEVs (supplementary material, Figure S3, right). We have previously shown that a combination of anti-VEGF therapy and immune checkpoint blockade with a specific antibody against PD-L1 is highly effective in stimulating HEVs and antitumour immunity in preclinical models of neuroendocrine pancreatic and breast cancer, but not NFpp10-GBM [29]. Here, we tested whether triple therapy consisting of LIGHT–CGKRK, anti-VEGF and anti-PD-L1 (Figure 5A) would potentiate LIGHT–CGKRK effects. Indeed, treatment of mice bearing GBM with triple therapy for 2 weeks increased the abundance of MECA79<sup>+</sup> CD31<sup>+</sup> double-positive vessels to 40% as compared with 20% in LIGHT–CGKRK single treatment groups (Figure 5B). This correlated with a six-fold to seven-fold



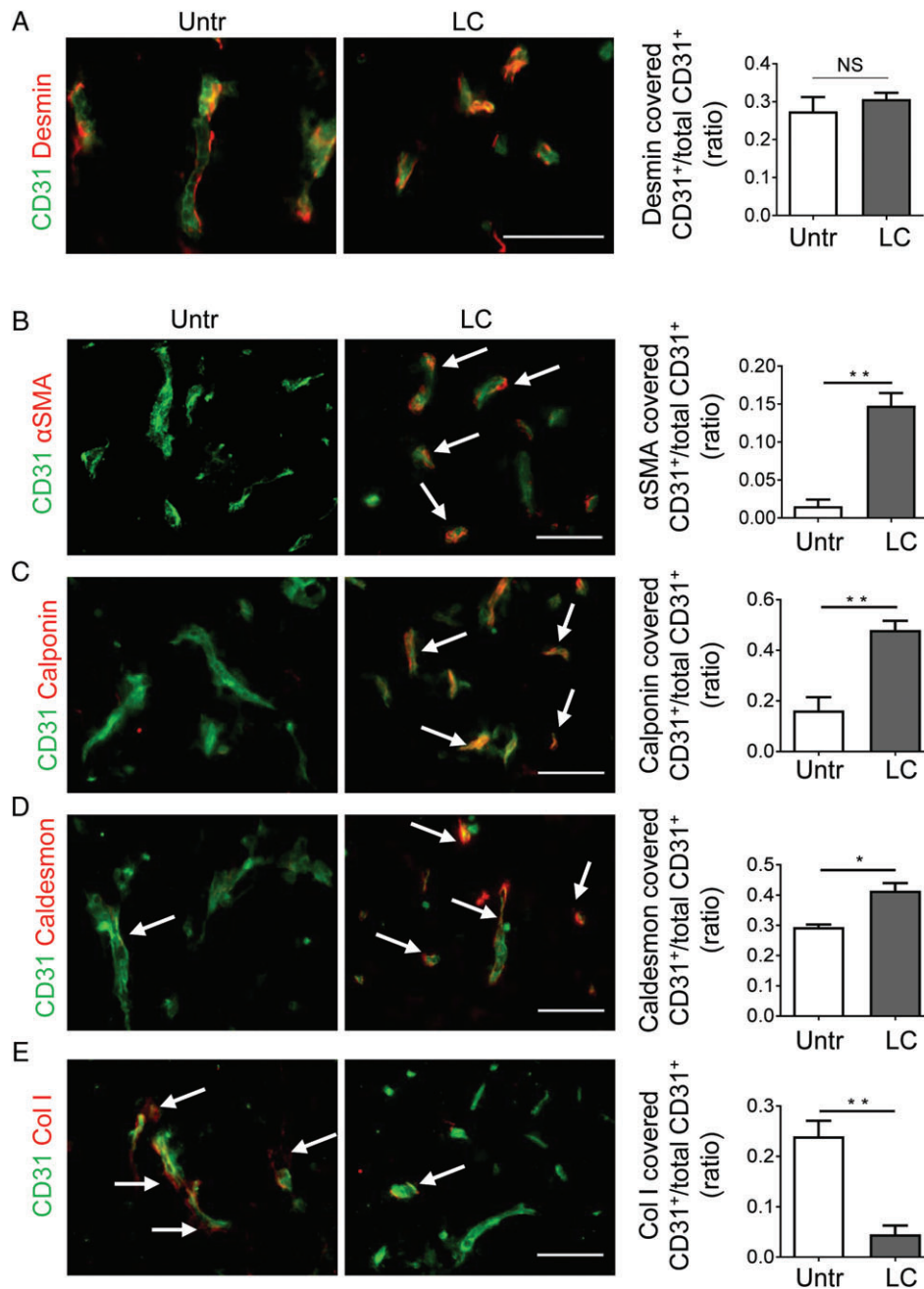


**Figure 3.** LIGHT–CGKRK treatment changes pericyte phenotype without affecting pericyte numbers around GBM blood vessels. (A–E) NFpp10–GBM mice were treated with 20 ng of LIGHT–CGKRK (LC) for 2 weeks or left untreated (Untr). Tumours were analysed by IHC to quantify the coverage of endothelial cells (CD31, green) by pericytes expressing (A) the pericyte-specific marker desmin (red), or the contractile markers (B)  $\alpha$ -SMA ( $n = 3$ ,  $**p = 0.002$ ), (C) calponin ( $n = 3$ ,  $**p = 0.008$ ), and (D) caldesmon ( $n = 3$ ,  $*p = 0.012$ ) or (E) the synthetic marker collagen I (Col I) ( $n = 3$ ,  $**p = 0.006$ ). Student's *t*-test. Arrows depict some blood vessels covered by overlapping markers (yellow). Scale bars: 50  $\mu$ m. NS, not statistically significant.

increase in the number of CD3<sup>+</sup> tumour-infiltrating T cells (Figure 5C). Both CD8<sup>+</sup> and CD4<sup>+</sup> T cells were increased in abundance (Figure 5D; supplementary material, Figure S4A), and T-cell infiltration was accompanied by upregulation of granzyme B (GrzB) expression and downregulation of FoxP3 expression (Figure 5E; supplementary material, Figure S4B). These findings were taken to imply that LIGHT–CGKRK synergizes with combination treatments to attract cytotoxic effector T cells into brain cancer. This was supported by a significantly reduced tumour burden, as quantified

by green fluorescent protein (GFP)<sup>+</sup> NFpp10 tumour cells in the brain, following 2 weeks of treatment with LIGHT–VTP ( $p = 0.04$ ) or triple therapy ( $p = 0.002$ ), as compared with untreated GBM (Figure 5F).

#### VTPs efficiently bind to human GBM

VTPs have been extensively tested for vascular targeting in murine syngeneic and xenograft cancer models [14]. To investigate VTP binding activity in human brain malignancies, we analysed freshly resected patient

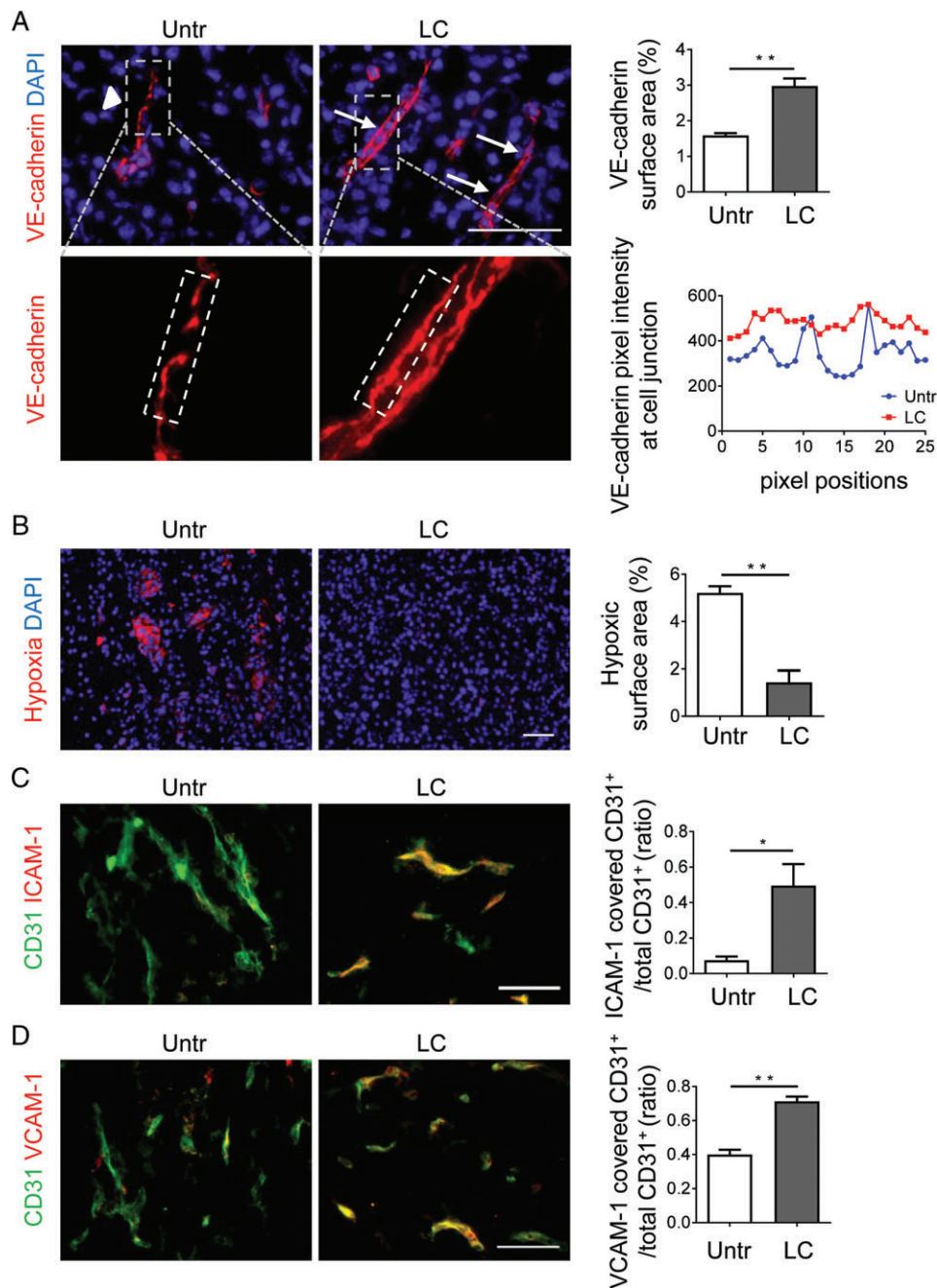


**Figure 4.** LIGHT–CGKRK treatment improves endothelial barrier integrity and vessel function. (A) NFpp10–GBM mice were left untreated (Untr) or treated for 2 weeks with LIGHT–CGKRK (LC). VE-cadherin expression in tumours was quantitatively (upper) and qualitatively (lower) assessed by IHC. Arrowheads point to gaps in disjointed adherens junctions, and arrows point to continuous VE-cadherin<sup>+</sup> adherens junctions;  $n=3$ ,  $**p=0.0032$ . Dashed outlines (grey, upper) indicate the areas enlarged below, and dashed white lines (below) indicate junctional areas quantified as VE-cadherin fluorescence (in pixels, same exposure for all groups) at various positions (horizontal axis) along the cell adherens junctions. (B) Assessment and quantification of intratumoural hypoxia by immunohistological detection of pimonidazole-positive areas (red) in treatment groups;  $n=3$ ,  $**p=0.0028$ . (C and D) Expression of ICAM-1 (C) or VCAM-1 (D) on GBM tumour vessels with and without LC treatment, analysed by IHC and quantified;  $n=3$ ,  $*p=0.027$ ,  $**p=0.0014$ . Student's *t*-test. Scale bars: 50  $\mu$ m.

biopsies from primary vascularized brain tumours of different origin, namely WHO grade IV astrocytoma and grade I meningioma (supplementary material, Table S1). Meningiomas arise from the membranous layer of the central nervous system, and constitute the second most common type of adult primary intracranial neoplasm. Although grade I meningiomas are angiogenic, they are normally slow-growing, and were employed in

this study as angiogenic, ‘benign’ tumours [44]. We first assessed CD105<sup>+</sup> blood vessel number and calibre in both tumour types (Figure 6A). The frequency of blood vessels and their lengths and diameters were found to be significantly increased in human GBM as compared with meningioma specimens ( $p \leq 0.02$ ; Figure 6B–D). Next, we examined the binding specificities of RGR, CGKRK or NGR for both GBM and meningioma.



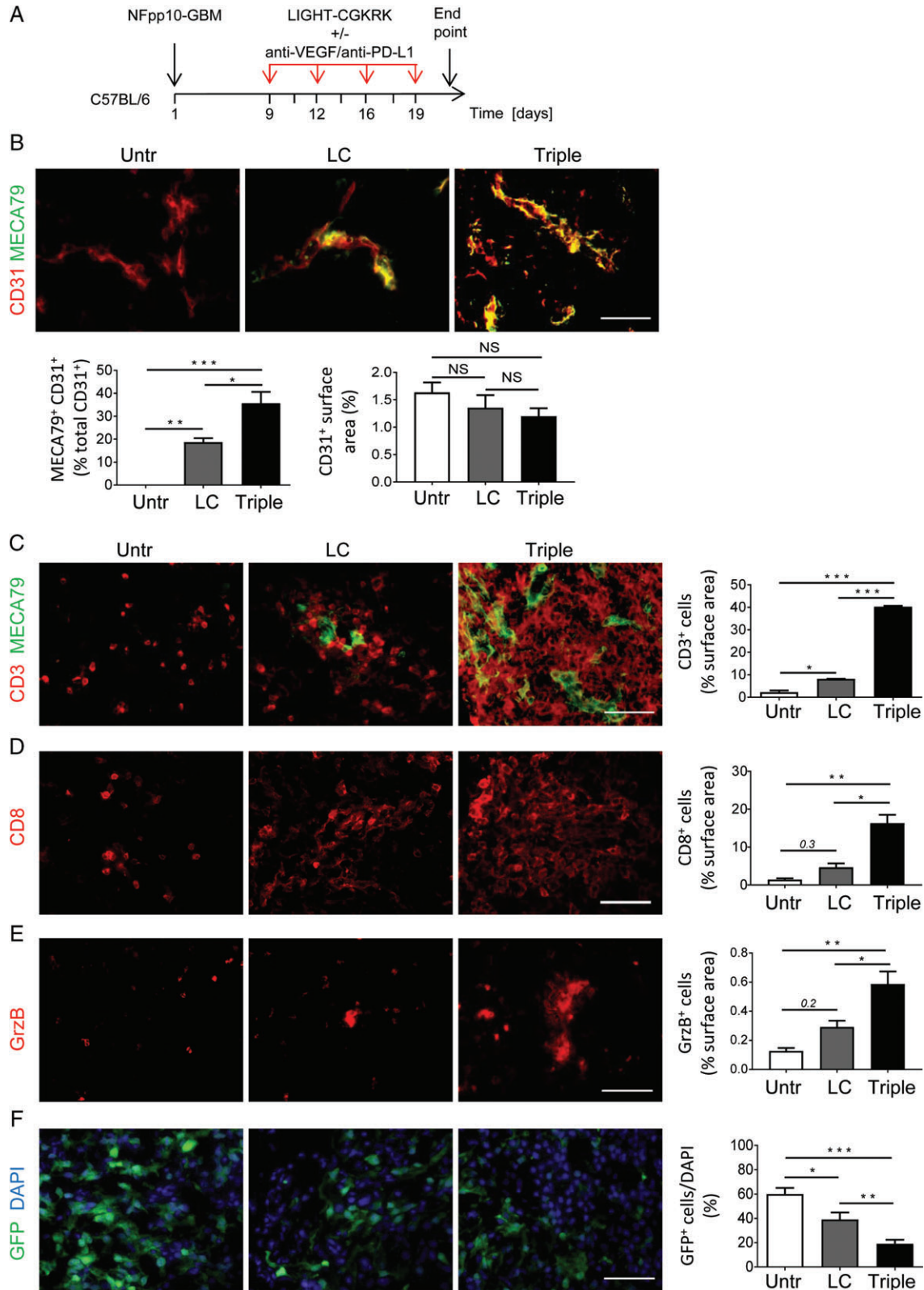


**Figure 5.** Induction of HEVs and T-cell infiltration by LIGHT-CGKRK is further amplified with combination immunotherapy. (A) LIGHT-CGKRK or triple treatment (LIGHT-CGKRK + anti-VEGF + anti-PD-L1) scheme in C56BL/6 mice harbouring established NFpp10-GBM. (B) NFpp10-GBM mice were left untreated (Untr), or treated for 2 weeks with LIGHT-CGKRK (LC) as a single reagent or combined with anti-VEGF/anti-PD-L1 treatment (Triple). Tumours were analysed for the presence of the HEV marker MECA79 (green) and overlaid (yellow) with CD31<sup>+</sup> (red) endothelial cells and total CD31<sup>+</sup> vascularity;  $n=3$ ,  $*p=0.0086$ ,  $**p=0.0035$ ,  $***p<0.0001$ . (C) Treatment groups as in (A) were assessed by IHC for MECA79<sup>+</sup> HEVs (green) and CD3<sup>+</sup> T cells (red), and T-cell infiltration into tumours was quantified;  $n=3$ ,  $*p=0.023$ ,  $***p<0.0001$ . (D) Corresponding CD8<sup>+</sup> T-cell infiltration and quantification;  $n=3$ ,  $*p=0.003$ ,  $**p=0.0007$ . (E) GrzB<sup>+</sup> immune cells and quantification;  $n=3$ ,  $*p=0.02$ ,  $**p=0.003$ . (F) Imaging and quantification of GFP<sup>+</sup> NFpp10 tumour cells in brain (DAPI);  $n=3$ ,  $*p=0.05$ ,  $**p=0.04$ ,  $***p=0.002$ . ANOVA. Scale bars: 50  $\mu$ m. NS, not statistically significant.

FAM-labelled peptides were incubated with fresh frozen tumour sections and directly visualized by fluorescence microscopy in conjunction with the vascular marker CD105. Figure 6E (upper) shows that CGKRR and RGR bound to >80% of GBM blood vessels but not to tumour cells; NGR was associated with <20% of GBM vessels, demonstrating lower binding activity. Further amplification of NGR-FAM signals with anti-FITC antibody was required to detect NGR signals on CD105<sup>+</sup> tumour blood vessels, consistent with CD13 expression on all GBM vessels (supplementary material, Figure S5A,B). Only 20% of blood vessels were found to be covered by VTPs in meningiomas (Figure 6E, lower). Overall, these results provide proof of the concept that VTP targeting of highly angiogenic human GBM blood vessels, in particular with RGR and CGKRR peptides, is a viable approach that may be explored further to normalize brain tumour blood vessels and boost anticancer immunity.

## Discussion

Treatment of aggressive, highly angiogenic primary brain cancers remains a major challenge. Our study evaluated peptide-mediated targeting of brain tumour vessels, and the capacity of a newly developed reagent to improve vessel function and T-cell infiltration into GBM.

We found, in two different murine orthotopic GBM models, that the CGKRR peptide shows superior binding activity than peptides containing the RGR or NGR binding motifs. This is consistent with previous data showing that CGKRR effectively binds blood vessels in brain tumour xenograft models and is therapeutically active when delivered in a nanoparticle formulation together with a proapoptotic peptide [19].

In fresh human GBM specimens, both CGKRR and RGR targeted the majority of highly angiogenic vessels, thus demonstrating that peptide-mediated payload delivery into grade IV GBM is highly feasible. Peptide binding to grade I meningiomas was significantly lower, potentially correlating with less aggressive growth and angiogenic activity. Strong RGR binding to human GBM is a new finding, because RGR targeting studies have, until now, been limited to murine pancreatic neuroendocrine and breast cancers [15,25,36,42,45]. Our result therefore warrants further investigations to explore its full potential for clinical applications. NGR, which binds to a tumour-specific isoform of aminopeptidase N/CD13, has been used to target a variety of murine and human cancers, including GBM [17,46]. For instance, NGR-tagged quantum dots specifically accumulated in a rat C6 glioma model as demonstrated by *in vivo* imaging [46]. However, as CD13 is also expressed on C6 cancer cells, a lack of vascular homing may be masked by direct NGR binding to tumour cells. In contrast to human GBM, which shows strong vascular CD13 expression [47], blood vessels in our mouse GBM models are CD13-negative by IHC, indicating

low expression levels. Similarly, in a model of neuroendocrine pancreatic cancer, CD13 is downregulated during tumour progression, thus making NGR binding to tumour vessels less effective [48]. As cyclic NGR, when conjugated to TNF- $\alpha$ , is therapeutically more active than its linear counterpart, it is also possible that linear NGR, as employed throughout this study, has inferior tumour vessel binding activity [49].

Having identified CGKRR as the best-performing vessel-homing peptide for GBM, our subsequent functional studies were performed with a murine LIGHT–CGKRR fusion compound. Our data demonstrate that the brain tumour microenvironment is susceptible to LIGHT–CGKRR-mediated vessel normalization, which increases pericyte maturity. This supports the idea that the concept of pericyte phenotype switching in tumours, which was first described in pancreatic cancer [10], is also an integral part of brain tumour vessel normalization. Induction of a more mature pericyte state has long-lasting effects [10], and thus may address the limitations of transient vessel normalization with anti-VEGF/VEGF receptor therapy.

Tighter, less leaky and activated tumour vessels in murine GBM reduce hypoxia and also enable enhanced lymphocyte infiltration into tumours. In fact, vessel normalization and T-cell influx correlate with and may even be causally involved in HEV induction in LIGHT–CGKRR-treated GBM; this is an interesting phenomenon that has also been observed in models of pancreatic neuroendocrine and breast tumours with anti-VEGF and anti-PD-L1 combination treatment [29] and human cancer [50]. In contrast to pancreatic or breast cancer models, NFpp10-GBM mice are refractory to combined anti-angiogenic and anti-PD-L1 therapy [29]. We show here that LIGHT–CGKRR treatment alone facilitates HEV induction and cytotoxic T-cell infiltration, which can be significantly enhanced with triple therapy of LIGHT–CGKRR with anti-VEGF/anti-PD-L1. This effect is most likely mediated by intratumoural LIGHT–LT $\beta$ R engagement and, consistent with the reduction in tumour burden obtained with a 2-week treatment regimen, is expected to convey a survival advantage; treatment with agonistic LT $\beta$ R antibody also stimulates HEV formation and significantly reduces tumour burden in NFpp10-GBM mice [29]. Therefore, vascular targeting of LIGHT in GBM holds great promise for improving antitumour immunity locally when combined with immune-enhancing modalities. There is growing evidence that the brain is less immunologically privileged than previously thought, and that brain cancers can profit from systemic immunostimulation [51]. Although immunotherapy faces challenges in brain cancer patients, there are subsets of patients who respond to treatment. Our findings are thus significant in the context of ongoing clinical trials that combine anti-VEGF treatment with checkpoint blockade [52,53].

The data presented here encourage further exploration of LIGHT–VTP therapy for angiogenic tumours such as GBM, with potential multiple benefits, including blood

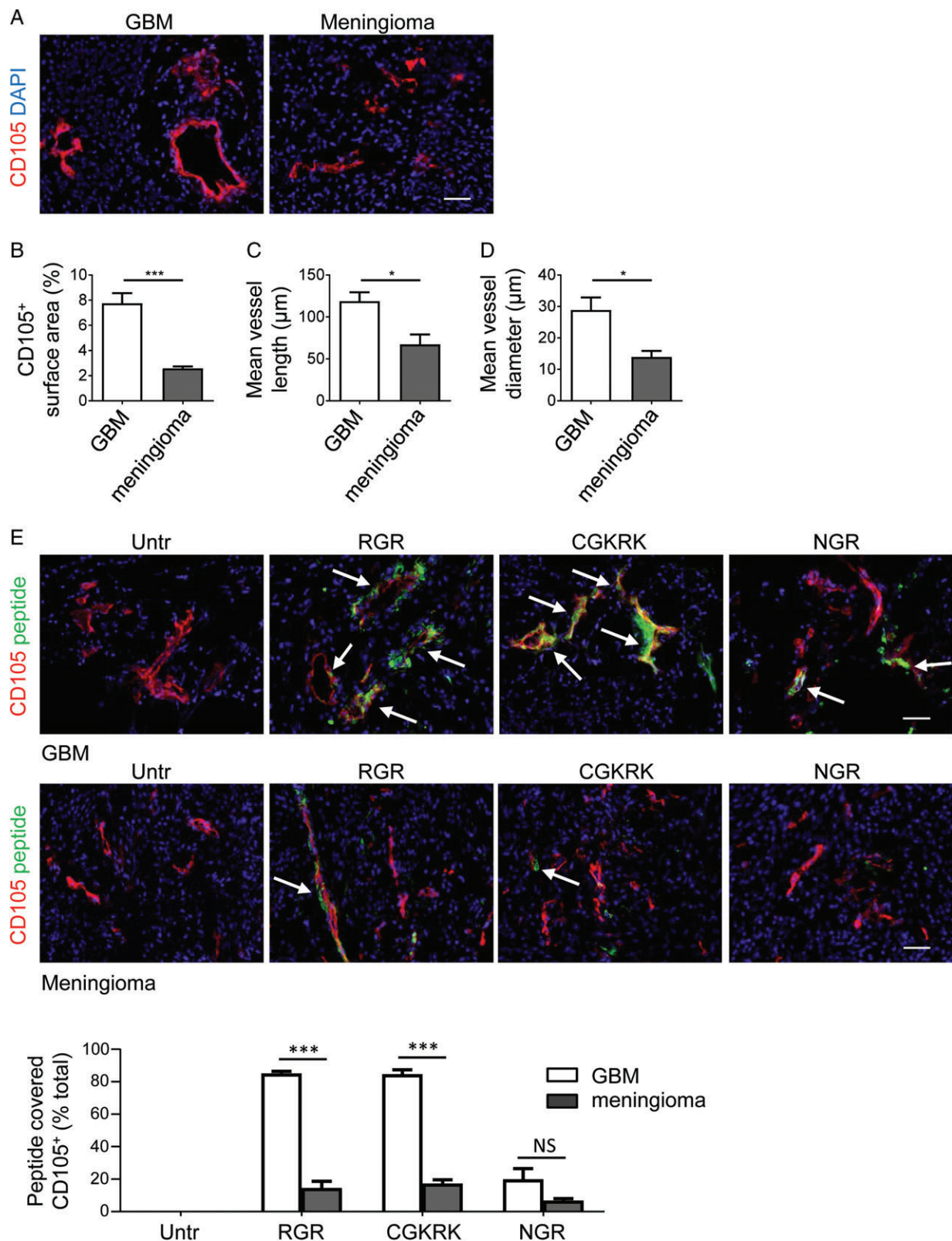


**Figure 6.** Peptide binding to human brain cancer blood vessels correlates with angiogenic activity. (A) Immunohistochemical analysis of CD105<sup>+</sup> tumour blood vessels (red) in grade IV GBM and grade I meningioma (for specimen details see Table 1). (B–D) Quantification of (B) overall vascularity (CD105<sup>+</sup> surface area) (\*\**p* = 0.0009), (C) mean vessel length (\**p* = 0.0133) and (D) mean vessel diameter (\**p* = 0.0213) in GBM (*n* = 6) and meningioma (*n* = 4). (E) Histological assessment of FAM-labelled RGR, CGKRK and NGR peptide (green) binding to CD105<sup>+</sup> (red) blood vessels in GBM (upper, *n* = 6) or meningioma (lower, *n* = 4), and quantification of peptide-covered vessels (yellow) (\*\**p* < 0.0001). Arrows depict some peptide-covered blood vessels. Student's *t*-test. Scale bars: 50 µm. NS, not statistically significant; Untr, untreated.



vessel normalization, oedema reduction and increases in immune cell infiltration and function via HEV induction.

## Acknowledgements

We thank M. Chopra (Harry Perkins Institute of Medical Research, Western Australia, Australia) for technical assistance, E. Ingley (Harry Perkins Institute of Medical Research, Western Australia, Australia) and J. Phillips (University of California, San Francisco, San Francisco, CA, USA) for reagents. This work was supported by the National Health and Medical Research Council of Australia (APP1042446 and APP1122108 to RG), the Cancer Council of Western Australia (APP1098579 to RG; Suzanne Cavanagh Early Career Funding to BH), the National Institutes of Health (R01CA188404 to GB), a Cancer Centre Support Grants Developmental Resource Allocation Program Award to GB, and a Woodside Energy Fellowship to RG.

## Author contributions statement

The authors contributed in the following way: RG, GB, GL, AKN: study concept and design; BH, AJ, VS, AJP, RJ, JH, GL: performance of experiments and/or collection of specimens; IPM, VRK, AJP, JH: generation of reagents; BH, JH, RG: analysis and interpretation of data; RG, BH: writing of the manuscript. All authors reviewed the manuscript.

## References

- Jain RK, di Tomaso E, Duda DG, *et al.* Angiogenesis in brain tumours. *Nat Rev Neurosci* 2007; **8**: 610–622.
- Dietrich J, Rao K, Pastorino S, *et al.* Corticosteroids in brain cancer patients: benefits and pitfalls. *Expert Rev Clin Pharmacol* 2011; **4**: 233–242.
- Gilbert MR, Dignam JJ, Armstrong TS, *et al.* A randomized trial of bevacizumab for newly diagnosed glioblastoma. *N Engl J Med* 2014; **370**: 699–708.
- Chinot OL, Wick W, Mason W, *et al.* Bevacizumab plus radiotherapy-temozolomide for newly diagnosed glioblastoma. *N Engl J Med* 2014; **370**: 709–722.
- Bergers G, Hanahan D. Modes of resistance to anti-angiogenic therapy. *Nat Rev Cancer* 2008; **8**: 592–603.
- De Palma M, Lewis CE. Macrophage regulation of tumor responses to anticancer therapies. *Cancer Cell* 2013; **23**: 277–286.
- Lu-Emerson C, Snuderl M, Kirkpatrick ND, *et al.* Increase in tumor-associated macrophages after antiangiogenic therapy is associated with poor survival among patients with recurrent glioblastoma. *Neuro Oncol* 2013; **15**: 1079–1087.
- Batchelor TT, Sorensen AG, di Tomaso E, *et al.* AZD2171, a pan-VEGF receptor tyrosine kinase inhibitor, normalizes tumor vasculature and alleviates edema in glioblastoma patients. *Cancer Cell* 2007; **11**: 83–95.
- Jain RK. Antiangiogenesis strategies revisited: from starving tumors to alleviating hypoxia. *Cancer Cell* 2014; **26**: 605–622.
- Johansson-Percival A, Li ZJ, Lakhiani DD, *et al.* Intratumoral light restores pericyte contractile properties and vessel integrity. *Cell Rep* 2015; **13**: 2687–2698.
- Lu-Emerson C, Duda DG, Emblem KE, *et al.* Lessons from anti-vascular endothelial growth factor and anti-vascular endothelial growth factor receptor trials in patients with glioblastoma. *J Clin Oncol* 2015; **33**: 1197–1213.
- Ruoslahti E, Bhatia SN, Sailor MJ. Targeting of drugs and nanoparticles to tumors. *J Cell Biol* 2010; **188**: 759–768.
- Corti A, Pastorino F, Curnis F, *et al.* Targeted drug delivery and penetration into solid tumors. *Med Res Rev* 2012; **32**: 1078–1091.
- Johansson A, Hamzah J, Ganss R. License for destruction: tumor-specific cytokine targeting. *Trends Mol Med* 2014; **20**: 16–24.
- Joyce JA, Laakkonen P, Bernasconi M, *et al.* Stage-specific vascular markers revealed by phage display in a mouse model of pancreatic islet tumorigenesis. *Cancer Cell* 2003; **4**: 393–403.
- Arap W, Pasqualini R, Ruoslahti E. Cancer treatment by targeted drug delivery to tumor vasculature in a mouse model. *Science* 1998; **279**: 377–380.
- Curnis F, Sacchi A, Borgna L, *et al.* Enhancement of tumor necrosis factor alpha antitumor immunotherapeutic properties by targeted delivery to aminopeptidase N (CD13). *Nat Biotechnol* 2000; **18**: 1185–1190.
- Hoffman JA, Giraudo E, Singh M, *et al.* Progressive vascular changes in a transgenic mouse model of squamous cell carcinoma. *Cancer Cell* 2003; **4**: 383–391.
- Agemy L, Friedmann-Morvinski D, Kotamraju VR, *et al.* Targeted nanoparticle enhanced proapoptotic peptide as potential therapy for glioblastoma. *Proc Natl Acad Sci U S A* 2011; **108**: 17450–17455.
- Gregorc V, De Braud FG, De Pas TM, *et al.* Phase I study of NGR-hTNF, a selective vascular targeting agent, in combination with cisplatin in refractory solid tumors. *Clin Cancer Res* 2011; **17**: 1964–1972.
- Lorusso D, Scambia G, Amadio G, *et al.* Phase II study of NGR-hTNF in combination with doxorubicin in relapsed ovarian cancer patients. *Br J Cancer* 2012; **107**: 37–42.
- Yu P, Lee Y, Liu W, *et al.* Priming of naive T cells inside tumors leads to eradication of established tumors. *Nat Immunol* 2004; **5**: 141–149.
- Chang YH, Hsieh SL, Chao Y, *et al.* Proinflammatory effects of LIGHT through HVEM and LTbetaR interactions in cultured human umbilical vein endothelial cells. *J Biomed Sci* 2005; **12**: 363–375.
- Lu TT, Browning JL. Role of the lymphotoxin/LIGHT system in the development and maintenance of reticular networks and vasculature in lymphoid tissues. *Front Immunol* 2014; **5**: 47.
- Johansson-Percival A, He B, Li ZJ, *et al.* De novo induction of intratumoral lymphoid structures and vessel normalization enhances immunotherapy in resistant tumors. *Nat Immunol* 2017; **18**: 1207–1217.
- Girard JP, Moussin C, Forster R. HEVs, lymphatics and homeostatic immune cell trafficking in lymph nodes. *Nat Rev Immunol* 2012; **12**: 762–773.
- Martinet L, Garrido I, Filleron T, *et al.* Human solid tumors contain high endothelial venules: association with T- and B-lymphocyte infiltration and favorable prognosis in breast cancer. *Cancer Res* 2011; **71**: 5678–5687.
- Martinet L, Le Guellec S, Filleron T, *et al.* High endothelial venules (HEVs) in human melanoma lesions: major gateways for tumor-infiltrating lymphocytes. *Oncol Immunology* 2012; **1**: 829–839.
- Allen E, Jabouille A, Rivera LB, *et al.* Combined antiangiogenic and anti-PD-L1 therapy stimulates tumor immunity through HEV formation. *Sci Transl Med* 2017; **9**: eaak9679.
- Reardon DA, Gokhale PC, Klein SR, *et al.* Glioblastoma eradication following immune checkpoint blockade in an orthotopic, immunocompetent model. *Cancer Immunol Res* 2016; **4**: 124–135.
- Lu KV, Chang JP, Parachoniak CA, *et al.* VEGF inhibits tumor cell invasion and mesenchymal transition through a MET/VEGFR2 complex. *Cancer Cell* 2012; **22**: 21–35.

32. Friedmann-Morvinski D, Bushong EA, Ke E, *et al.* Dedifferentiation of neurons and astrocytes by oncogenes can induce gliomas in mice. *Science* 2012; **338**: 1080–1084.
33. Du R, Lu KV, Petritsch C, *et al.* HIF1 $\alpha$  induces the recruitment of bone marrow-derived vascular modulatory cells to regulate tumor angiogenesis and invasion. *Cancer Cell* 2008; **13**: 206–220.
34. Agemy L, Sugahara KN, Kotamraju VR, *et al.* Nanoparticle-induced vascular blockade in human prostate cancer. *Blood* 2010; **116**: 2847–2856.
35. Sugahara KN, Teesalu T, Karmali PP, *et al.* Tissue-penetrating delivery of compounds and nanoparticles into tumors. *Cancer Cell* 2009; **16**: 510–520.
36. Johansson A, Hamzah J, Payne CJ, *et al.* Tumor-targeted TNF $\alpha$  stabilizes tumor vessels and enhances active immunotherapy. *Proc Natl Acad Sci U S A* 2012; **109**: 7841–7846.
37. Armulik A, Genove G, Mae M, *et al.* Pericytes regulate the blood–brain barrier. *Nature* 2010; **468**: 557–561.
38. Mazzone M, Dettori D, Leite de Oliveira R, *et al.* Heterozygous deficiency of PHD2 restores tumor oxygenation and inhibits metastasis via endothelial normalization. *Cell* 2009; **136**: 839–851.
39. Cantelmo AR, Conradi LC, Brajic A, *et al.* Inhibition of the glycolytic activator PFKFB3 in endothelium induces tumor vessel normalization, impairs metastasis, and improves chemotherapy. *Cancer Cell* 2016; **30**: 968–985.
40. Zhao Y, Ting KK, Li J, *et al.* Targeting vascular endothelial-cadherin in tumor-associated blood vessels promotes T-cell-mediated immunotherapy. *Cancer Res* 2017; **77**: 4434–4447.
41. Dirx AE, oude Egbrink MG, Castermans K, *et al.* Anti-angiogenesis therapy can overcome endothelial cell anergy and promote leukocyte–endothelium interactions and infiltration in tumors. *FASEB J* 2006; **20**: 621–630.
42. Hamzah J, Altin JG, Herrington T, *et al.* Targeted liposomal delivery of TLR9 ligands activates spontaneous antitumor immunity in an autochthonous cancer model. *J Immunol* 2009; **183**: 1091–1098.
43. Shrimali RK, Yu Z, Theoret MR, *et al.* Antiangiogenic agents can increase lymphocyte infiltration into tumor and enhance the effectiveness of adoptive immunotherapy of cancer. *Cancer Res* 2010; **70**: 6171–6180.
44. Barresi V. Angiogenesis in meningiomas. *Brain Tumor Pathol* 2011; **28**: 99–106.
45. Hamzah J, Nelson D, Moldenhauer G, *et al.* Vascular targeting of anti-CD40 antibodies and IL-2 into autochthonous tumors enhances immunotherapy in mice. *J Clin Invest* 2008; **118**: 1691–1699.
46. Huang N, Cheng S, Zhang X, *et al.* Efficacy of NGR peptide-modified PEGylated quantum dots for crossing the blood–brain barrier and targeted fluorescence imaging of glioma and tumor vasculature. *Nanomedicine* 2017; **13**: 83–93.
47. Di Matteo P, Arrigoni GL, Alberici L, *et al.* Enhanced expression of CD13 in vessels of inflammatory and neoplastic tissues. *J Histochem Cytochem* 2011; **59**: 47–59.
48. Porcellini S, Asperti C, Valentinis B, *et al.* The tumor vessel targeting agent NGR-TNF controls the different stages of the tumorigenic process in transgenic mice by distinct mechanisms. *Onc Immunology* 2015; **4**: e1041700.
49. Colombo G, Curnis F, De Mori GM, *et al.* Structure–activity relationships of linear and cyclic peptides containing the NGR tumor-homing motif. *J Biol Chem* 2002; **277**: 47891–47897.
50. Hiraoka N, Ino Y, Yamazaki-Itoh R, *et al.* Intratumoral tertiary lymphoid organ is a favourable prognosticator in patients with pancreatic cancer. *Br J Cancer* 2015; **112**: 1782–1790.
51. Fecci PE, Heimberger AB, Sampson JH. Immunotherapy for primary brain tumors: no longer a matter of privilege. *Clin Cancer Res* 2014; **20**: 5620–5629.
52. McGranahan T, Li G, Nagpal S. History and current state of immunotherapy in glioma and brain metastasis. *Ther Adv Med Oncol* 2017; **9**: 347–368.
53. Carter T, Shaw H, Cohn-Brown D, *et al.* Ipilimumab and bevacizumab in glioblastoma. *Clin Oncol (R Coll Radiol)* 2016; **28**: 622–626.

## SUPPLEMENTARY MATERIAL ONLINE

### Supplementary figure legends

**Figure S1.** Murine GBM lack CD13 expression and NGR binding

**Figure S2.** LIGHT-CGKRR treatment increased tumour perfusion

**Figure S3.** Intratumoral T cells clustered around HEVs but not CD31<sup>+</sup> endothelia

**Figure S4.** Increased CD4<sup>+</sup> T cell infiltration correlated with reduced intratumoral FoxP3 signals

**Figure S5.** NGR-FAM binding to human GBM blood vessels correlated with CD13 expression

**Table S1.** Patient information and histopathology